PARISFOG: Shedding New Light on Fog Physical Processes

M. Haeffelin, Thierry Bergot, T. Elias, R. Tardiff, Dominique Carrer, P. Chazette, M. Colomb, P. Drobinski, E. Dupont, J.-C. Dupont, et al.

PARISFOG

Shedding New Light on Fog Physical Processes

BY M. HAEFFELIN, T. BERGOT, T. ELIAS, R. TARDIF, D. CARRER, P. CHAZETTE, M. COLOMB, P. DROBINSKI, E. DUPONT, J.-C. DUPONT, L. GOMES, L. MUSSON-GENON, C. PIETRAS, A. PLANA-FATTORI, A. PROTAT, J. RANGOGNIO, J.-C. RAUT, S. RÉMY, D. RICHARD, J. SCIARE, AND X. ZHANG

A field experiment covering more than 100 fog and near-fog situations during the winter of 2006–07 investigated the dynamical, microphysical, and radiative processes that drive the life cycle of fog.

Low-visibility meteorological conditions, such as fog, are not necessarily considered extreme weather conditions, such as those encountered in storms, but their effects on society can be just as significant. Fog creates situations where our transportation systems on roads, rails, sea, and air become more hazardous, requiring specific safety measures to prevent accidents that lead to delays or cancellation of transport. While the meteorological event is inevitable, there is significant pressure from airport and road transport authorities to obtain more reliable forecasts. Local short-term fog forecasts relying on 1D assimilation-forecast high-resolution models (e.g., Cobel-Isba model; Bergot et al. 2005) have been implemented at airports in Paris and Lyon, France (Bergot 2007), and San Francisco, California (Ivaldi et al. 2006). These models include precise parameterizations of radiative, turbulent, and surface processes and rely on detailed and continuous near-surface observations of temperature, humidity, wind, radiation, and visibility. They produce more accurate fog forecasts than current NWP models (Bergot 2007), but their application remains local. Hence further improvements in fog forecast rely on better understanding of physical processes at play in the fog life cycle.

Fog formation results from condensation of water vapor into liquid droplets or ice crystals, as a result of air cooling, moistening, and/or through mixing of contrasting air parcels. The most common scenario considered when invoking fog formation over land involves ▶

Aerosol and fog microphysics sensors are used to further document particular events of fog and near-fog. For more information see Fig. 3.

nocturnal radiative cooling under light wind conditions (Roach 1995), while dissipation typically occurs a few hours after sunrise as a result of warming from sensible heat fluxes over a surface heated by solar radiation (the so-called fog burn-off). However, this statement hides a more complex reality, with regions experiencing fog events due to conditions such as advection fog or stratus lowering rather than the typical radiative fog event (Croft et al. 1997; Tardif and Rasmussen 2007). Furthermore, the nature and concentration of aerosols present in the surface layer are known to be critical parameters throughout the fog life cycle as their chemical and microphysical properties control the activation process (Rangognio et al. 2009), and their optical properties affect radiative cooling and heating (Elias et al. 2009). In addition, turbulent mixing is known to be a key but ambiguous factor in influencing fog formation. If turbulent mixing is too low, dew deposition at the surface will inhibit condensation in the atmosphere and hence inhibit fog formation. If turbulence is strong enough, it may promote condensation in a supersaturated surface layer of sufficient depth and hence lead to fog formation and development (Bergot et al. 2008).

As reviewed in Gultepe et al. (2007), several field campaigns carried out in Europe and North America have focused on physical and chemical processes involved in continental fog. Early studies revealed that the development of radiation fog results from the balance between radiative cooling and turbulent mixing [e.g., Roach et al. (1976) based on observations performed in Cardington, United Kingdom]. Other datasets were put together to focus on radiation fog such as the Fog-82 campaign in Albany, New York (Meyer et al. 1986), and the Lille-88 and Lille-91 field experiments in northern France (Guédalia and Bergot 1994). The role of turbulence was investigated using measurements performed at the Cabauw experimental site in the Netherlands (Duynkerke 1991, 1999). In the same period, the Po Valley in northern Italy received considerable attention, with two field campaigns (1989 and 1994) focused on fog microphysical processes and evolution of chemical species (Fuzzi et al. 1992, 1998).

However, the occurrence and development of fog is the result of multiple processes occurring simultaneously that interact nonlinearly with each other. These interactions likely result in nontrivial sets of key fog parameter values leading to fog formation, while other combinations of values prevent fog formation. Today key remaining questions are the following: How do competing radiative, thermodynamic, microphysical, dynamical, and chemical processes interact with each other? Do key parameters such as aerosol concentration, supersaturation, radiative cooling rates, and turbulent mixing take on critical values to reach a particular balance that result in fog formation? Is there a hierarchy in these processes, or a single dominating process whose behavior must be better quantified? The significant variability of local conditions in which fog formation, vertical development, and dissipation typically occur emphasizes the difficulty of giving complete answers to these questions.

The ParisFog field experiment was designed to shed some light on these questions by 1) monitoring simultaneously all important processes and 2) sampling a large range of conditions during a 6-month winter season (October 2006–March 2007). To do so, the experimental setup was designed to monitor on a routine basis surface conditions, large- and small-scale dynamics, radiation, turbulence, precipitation, droplet and aerosol microphysics, and aerosol chemistry, combining in situ and remote sensing instruments on a long-term basis to describe the complete environment in which fog develops. The long observing period was intended to sample processes taking place during contrasting scenarios, such as fog formation versus nonformation in similar conditions (quasi fog), formation in clean and polluted air masses, and evolution of different fog types.

AFFILIATIONS: Haeffelin and Dupont—Institut Pierre-Simon Laplace, Ecole Polytechnique, Palaiseau, France; Bergot, Tardif, Carrer, Gomes, Rangognio, and Rémy—CNRM-GAME, Météo-France, Toulouse, France; Drobinski and Pietras—Laboratoire de Météorologie Dynamique, Institut Pierre-Simon Laplace, Palaiseau, France; Musson-Genon, Dupont, and Zhang—Centre d'Enseignement et de Recherches en Environnement Atmosphérique (Laboratoire Commun ENPC—EDF R&D), Chatou, France; Colomb—Laboratoire Régional des Ponts et Chaussées, Clermont-Ferrand, France; Chazette, Elias, and Sciare—Laboratoire des Sciences du Climat et de l'Environnment/IPSL, Saclay, France; Plana-Fattori, Protat, and Raut—Laboratoire Atmosphères, Milieux, Observations Spatiales, Guyancourt, France; Richard—Institut Physique du Globe de Paris, Paris, France
CORRESPONDING AUTHOR: Martial Haeffelin, Institut Pierre-Simon Laplace, LMD/IPSL, Ecole Polytechnique, 91128 Palaiseau CEDEX, France
E-mail: martial.haeffelin@ipsl.polytechnique.fr

The abstract for this article can be found in this issue, following the table of contents.
DOI:10.1175/2009BAMS2671.1

In final form 1 December 2009

This paper presents the 6-month ParisFog field experiment and provides information on the ParisFog database. It describes the noteworthy meteorological and physical conditions encountered and illustrates key processes involved in various fog types using ParisFog observations.

PARISFOG OBSERVATIONS AND DATABASE. The geographical location of Paris, France, was chosen because fog creates strong constraints on transport in an area of 12 million inhabitants with two large international airports and a heavily used road traffic system. The Paris area benefits from a rich observation network operated by Météo-France, with 29 surface weather stations, 7 locations where visibility and cloud-base height are monitored at national and regional airports, and an operational radiosonde station. The area also hosts the Site Instrumental de Recherche en Télédétection Atmosphérique (SIRTA) atmospheric remote sensing observatory (Haeffelin et al. 2005) located 25 km south of the Paris city center, as shown in Fig. 1.

To document simultaneously all key processes involved in the life cycle of fog, a suite of remote sensing and in situ sensors from 10 French research laboratories was deployed on three different zones of the SIRTA observatory in a 4-km^2 surface area. Zone 1, gathering most instruments, was characterized by small-scale heterogeneities such as a lake, an open field, and a small wood (Fig. 1). Zone 2 was characterized by a high concentration of 2–3-story buildings. Zone 3 was more than 1 km away from any significant building. Table 1 lists the instruments deployed during the field experiment and parameters that can be retrieved from their measurements. As fog events in France can be clustered during a few weeklong periods or occur sporadically throughout fall, winter, and spring, the experimental setup strived to deploy a majority of instruments capable of operating on a continuous and unattended basis (depicted in Fig. 2). Particular events of fog and near-fog were further documented by deploying additional, albeit more user-intensive, sensors during intensive observation periods (IOPs), as shown in Fig. 3.

Two 30-m masts, located in zones 1 and 3, hosted standard weather sensors to monitor the vertical thermodynamic structure in the surface layer. Measurements were extended vertically by radiosonde profiles performed routinely at 0000 and 1200 UTC 15 km west of SIRTA as part of the Météo-France national network. During IOPs, measurements were also extended using thermodynamic sensors on a tethered balloon (temperature, humidity, and wind measurements at five levels covering the 30–150-m altitude range) and radiosondes launched from the site every 3 h. Thermal and moisture soil conditions were monitored down to 50-cm depth. A Bowen station was used to measure surface sensible and latent heat fluxes. Up- and downwelling solar and thermal radiative fluxes were measured in the three zones.

As local dynamic conditions are key in fog processes, wind and turbulence were monitored by several systems distributed in the 4-km^2 domain. Sonic anemometers at 10- and 30-m heights were available to study the state of turbulence. UHF-radar profiler data were available to monitor the vertical structure of the wind field.

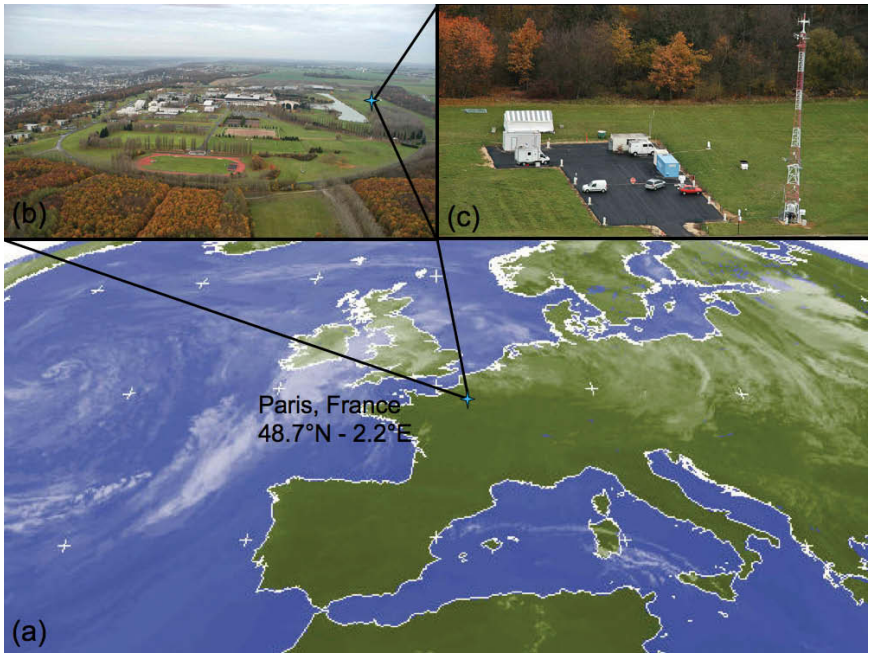

Fig. 1. The ParisFog field experiment took place at the SIRTA experimental site. (a) SIRTA is located 25 km south of Paris, France. (b) The experimental site consists of three observation zones on a 4 km^2 campus. (c) Zone 1 gathers remote-sensing and in situ sensors in a large open field.

Several systems were deployed to study the aerosol particle properties present during the fog life cycle. This setup included an aethalometer and a nephelometer to characterize absorption and scattering properties of particles, respectively. It included several particle size counters to cover the nano- to micrometer particle size range. Filter sampling were done prior to, during, and after several fog events to analyze the presence of black carbon and hydrophilic particles such as sulfates. The setup was designed to monitor macrophysical properties of fog layers using a visibility meter for horizontal visibility, a ceilometer to monitor cloud and fog base height, and a 95-GHz Doppler radar for cloud- and fog-top height and vertical dynamics. Fog

Table 1. List of instruments deployed during ParisFog, parameters that can be retrieved from their measurements, instrument range (vertical range or, spectral range, as relevant) and resolution, and type of operations (RT: routine operations; IOP: operations during intensive observation periods).

Category	Instruments	Measured parameters	Range and resolution	Operations
Ground and surface properties	Ground temperature and moisture sensors located at 0, –10, –20, –30, –50 cm	Temperature and water profile in the ground.	RA: 0 to –50 cm RE: 1 min	RT
	Bowen station	Surface energy budget (sensible + latent).	—	RT
Surface layer meteorology	Temperature and humidity sensors located at 1, 2, 5, 10, and 30 m on two 30-m masts located 1 km apart	Temperature and humidity profiles at five levels above ground.	RA: 1–30 m RE: 1 min	RT
	PTUV sensors located at 2 and 10 m (zone 1); 17 and 25 m (zone 2)	Pressure, temperature, humidity, wind speed and direction, and precipitation.	RA: 1–30 m RE: 1 min	RT
	Young and Gill sonic anemometers located at 10 and 30 m on two 30-m masts located 1 km apart	Turbulent kinetic energy, friction velocity u^*.	RA: 10–30 m RE: 10 min	RT
Radiative fluxes	Kipp & Zonen CH1, CM22, and CG4 radiometers (zone 2)	Downwelling shortwave (SW) direct, diffuse, and global + longwave (LW) irradiances.	RA: surface RE: 1 min	RT
	Kipp & Zonen CM21 and CG2 radiometers (zone 1) at 2 and 30 m	Downwelling and upwelling SW and LW global irradiances.	RA: 2–30 m RE: 1 min	RT
Atmospheric profiles	PTUV sondes (Vaisala) attached to a tethered balloon at 50, 70, 90, 110, and 130 m	Pressure, temperature, humidity, wind speed, and direction (50–130 m).	RA: 50–130 m RE: 1 min	IOP
	RS90 radiosondes launched at 0000 and 1200 UTC, 15 km from zone 1	Pressure, temperature, humidity, wind speed, and direction (0–20 km).	RA: 0–20 km RE: 2 day^{-1}	RT
	RS92 radiosonde launched during IOPs from zone 1	Pressure, temperature, humidity, wind speed, and direction (0–20 km).	RA: 0–20 km RE: 2–6 IOP^{-1}	IOP
Aerosol and fog optical properties	Degreanne DF320 and DF20+ visibilimeter (490–750 nm, 550 nm peak sensitivity)	Visibility at 4-m height at two locations 1 km apart.	RA: surface RE: 10 s	RT
	Vaisala CT25K ceilometer (905 nm)	Vertical profile of backscatter. Fog and cloud-base height.	RA: 0.1–5 km RE: 1 min	RT
	7I aethalometer	Absorption coefficient	RA: surface RE: 1 min	RT
	TSI 3563 nephelometer	Scattering coefficient (10°–170°) at 450, 550, and 700 nm	RA: surface RE: 1 min	RT
	CIMEL CE-318 sun photometer (440, 670, 870, 1020 nm)	Aerosol optical depth.	RA: column integrated RE: 15 min	RT

droplet size distribution was monitored at 2 m by a Palas particle counter.

Fog presence and visibility were monitored in a 200-km area around Paris using an experimental product from Météo-France based on Meteosat Second Generation measurements and a regional network of visibility meters (Guidard and Tzanos 2007). The ParisFog database now contains 3,000 h of high-temporal-resolution routine measurements. Raw data are available at very high temporal resolutions; 10 Hz to 10 min depending on the parameters. Processed data are available at 10- or 30-min time steps. The ParisFog database can be accessed through a dedicated Web site (http://parisfog.sirta.fr).

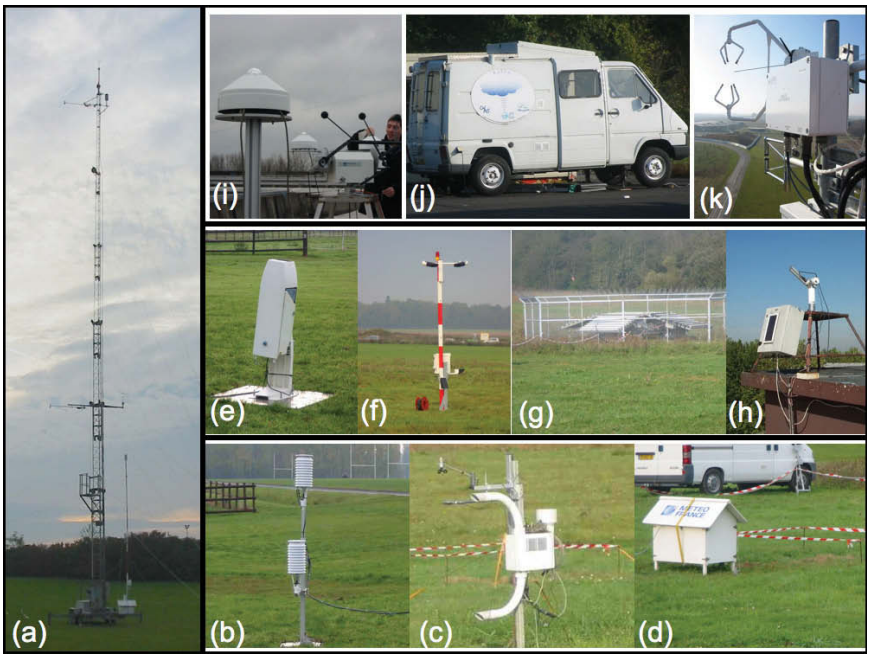

Fig. 2. Instruments deployed during the ParisFog field experiment operating on a routine basis: (a), (b) Standard pressure, temperature, humidity, and wind sensors from 1 to 30 m; (c) surface flux station using Bowen ratio; (d) soil temperature and moisture profiles; (e) Vaisala CT25K ceilometer; (f) Degreanne visibilimeter; (g) Degreanne UHF wind profiling radar; (h) CIMEL sun photometer; (i) solar and thermal radiative flux station; (j) 95-GHz Doppler cloud radar; (k) sonic anemometers at 10- and 30-m heights.

Table 1. Continued.

Category	Instruments	Measured parameters	Range and resolution	Operations
Aerosol and fog microphysics	Palas Welas-2000 particle counter	Aerosol and fog particle size distribution in 0.4–10-micron range	RA: 0.4–10 microns	IOP
			RE: 5 min	
	TSI Scanning Mobility Particle Sizer (SMPS) particle counter	Aerosol particle size distribution in 0.01–0.4-micron range	RA: 0.01–0.4 microns	RT
			RE: 10 min	
	GRIMM condensation particle counter (CPC)-5400 particle counter	Aerosol particle counter	RA: 0.01–0.4 microns	RT
			RE: 1 min	
Aerosol chemistry	0.4- and 8-nm filters + spectrometer analysis	Concentration of BC and major ions (sulfates, nitrates, ammonium)	RA: surface	IOP
			RE: 2 IOP^{-1}	
Ancillary remote sensing	Thales GPS receiver	Column-integrated precipitable water	RA: column	RT
			RE: 15 min	
	Degreanne UHF radar	Vertical profile of wind speed and direction	RA: 500–2000 m	RT
			RE: 15 min	
	95-GHz Doppler radar	Vertical profile of reflectivity and Doppler velocity. Cloud boundaries. Microphysics of ice.	RA: 100 m–15 km	
			RE: 1 min	RT

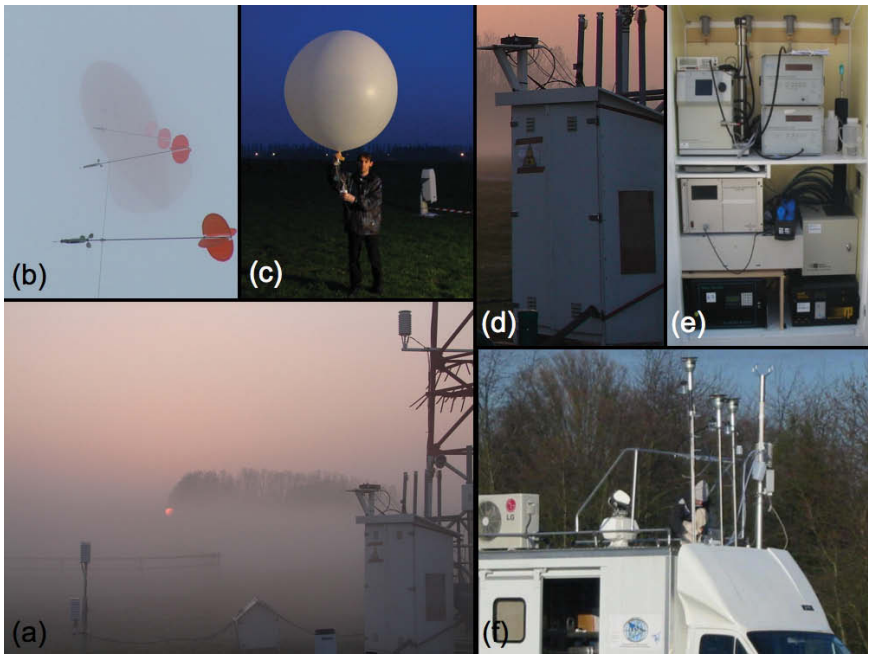

Fig. 3. (a) Instruments deployed and operated during situations favorable for fog formation; (b) tethered balloon with pressure, temperature, humidity, and wind sensors at five levels; (c) RS92 radiosonde launched during IOPs; (d), (e) aerosol and fog microphysics sensors (see Table 1 for details).

PARISFOG: OVER 100 FOG AND NEAR-FOG SITUATIONS. Routine surface meteorological observations (surface visibility, ceilometer cloud base, near-surface temperature, humidity, wind, and precipitation) collected during the entire experiment were analyzed to identify and characterize fog and near-fog (sometimes referred to as mist) events by adapting the methodology presented in Tardif and Rasmussen (2007) to the higher-frequency ParisFog observations. Events were defined as sufficiently long sequences with a majority of visibility observations below the standard 1 km threshold for fog and below 5 km but remaining above 1 km for near fog. A subset of near-fog events was labeled "quasi-fog" events when visibilities reached values below 2 km but remained above the 1-km fog threshold (see Table 2 for summary of definitions). Events were identified whenever the 10-min-averaged visibility reached values below corresponding thresholds during at least 30 min over a 50-min time window (3 out of 5 values). The end of a fog event took place whenever the 3-out-of-5 rule was no longer verified, including at least one visibility observation above 2 km. Near-fog events ended simply when surface visibility increased back above 5 km for a period equal to or longer than 30 minutes.

Completing the analysis, the classification algorithm of Tardif and Rasmussen (2007) was used to determine a fog type for every fog event, with five types considered: radiation fog (resulting from surface cooling under mostly clear skies), advection fog (sudden reduction in visibility under a significant wind speed), stratus lowering (prior presence of a low cloud layer with a gradual lowering of its base as detected by the ceilometer), precipitation fog (presence of stratiform rain at onset as described

Table 2. Definitions for fog, mist, near-fog, and quasi-fog events.

Terms	Definition from AMS glossary of meteorology (Glickman 2000).	Definition for the purpose of this study
Fog	Water droplets suspended in the atmosphere in the vicinity of the Earth's surface that reduce visibility below 1 km	10-min-averaged visibility remains below 1 km during at least 30 minutes over a 50-min time window
Mist	A suspension in the air consisting of an aggregate of microscopic water droplets or wet hygroscopic particles (of diameter not less than 0.5 mm or 0.02 in.), reducing the visibility at the Earth's surface to not less than 1 km	(Not used in this study because it lacks precise upper boundary in visibility.)
Near fog	—	10-min-averaged visibility ranges between 1 and 5 km during at least 30 minutes over a 50-min time window
Quasi fog	—	10-min-averaged visibility ranges between 1 and 2 km during at least 30 minutes over a 50-min time window

in Tardif and Rasmussen 2008), and morning transition fog (onset after sunrise during the morning transition of the boundary layer). Events were labeled as *other* whenever conditions did not match the simple conceptual models used in the classification.

The analysis of routine SIRTA observations indicated that a total of 154 h of fog and 518 h of near fog (including 141 h of quasi fog) were distributed over 37 and 109 days, respectively, representing 20% of the total number of hours of the experiment. Even though winter 2006/07 was exceptionally warm in Paris and all of Europe—a +2.5°C anomaly in mean temperature according to Yiou et al. (2007)—the number of fog days was consistent with the 30-yr climatology for the area (corresponding to 28 fog days for the Orly Airport and 51 fog days for the Trappes Meteorological Center, located 5 km east and 15 km west of SIRTA, respectively) (Météo-France 2008). These hours of reduced visibility were distributed among a total of 36 fog and 89 near-fog (including 21 quasi-fog) events (Fig. 4). A large majority of these events were associated with anticyclonic large-scale weather conditions (Tables 3 and 4), typical of both radiation and stratus-lowering fog scenarios (e.g., Meyer and Lala 1990; Wobrock et al. 1992), each type representing about 40% of all fog events. The more marginal fog types, corresponding to two advection fog events, a morning transition fog, and one precipitation fog event, occurred during short-lived anticyclonic or perturbed weather conditions. Three other events for which a fog type could not be determined with confidence also occurred during the experiment.

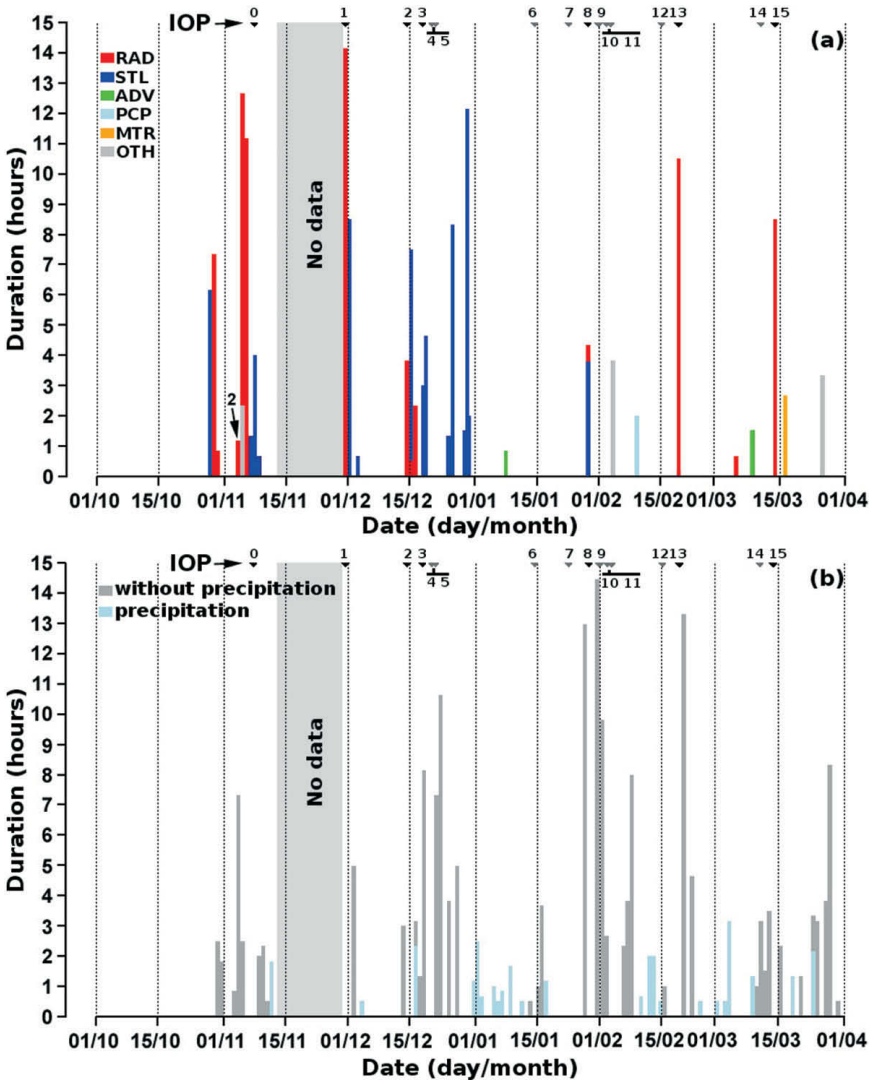

Fig. 4. Temporal distribution of (a) fog events of various types (RAD: radiation; STL: stratus lowering; ADV: advection; PCP: precipitation; MTR: morning transition; OTH: other), (b) near-fog events and their duration (y axis).

Illustrating the complexity of fog formation during ParisFog, the evolution of near-surface temperature leading to onset is shown in Fig. 5 for every fog event of the experiment. Cooling trends tend to be better defined for radiation fog events but still with a considerable variability in intensity. More subtle temperature trends, but predominantly cooling, characterize stratus-lowering events. Few occurrences of fog formation took place under warming temperatures, indicating the dominating influence of moistening leading to onset in these cases.

Among the quasi-fog events, nearly half took place under clear skies due to aerosol hygroscopic growth in increasing relative humidity conditions related to radiative cooling, while the other half took place under low cloud bases not quite reaching the surface (Table 4). Three cases, two with low ceilings and one in clear sky, were even characterized by brief periods

Table 3. Summary of fog events, with the date and time of the event onset, fog type (RAD: radiation; STL: stratus lowering; ADV: advection; PCP: precipitation; MTR: morning transition; OTH: other), time of fog formation relative to sunset and sunrise, dissipation with respect to sunrise (–: before, +: after), lowest visibility observed during the event, and synoptic weather classification (H: anticyclonic, L: cyclonic, T: transition). An asterisk indicates an event occurring on the same night as the previous event.

No.	Date/time (day/month/year h:min)	Fog type	Formation (hour to sunset/sunrise)	Dissipation (hour to sunrise)	Lowest visibility (km)	Synoptic weather
1	27/10/2006 01:50	STL	+9.3/−4.8	+1.4	0.09	H
2	28/10/2006 01:00	RAD	+8.5/−5.7	+1.7	0.09	H
3	29/10/2006 17:40	RAD	+1.2/−13.0	−12.2	0.17	H
4	03/11/2006 21:50	RAD	+5.5/−9.0	−7.8	0.12	H
5	*03/11/2006 23:30	RAD	+7.2/−7.3	−6.2	0.14	H
6	*04/11/2006 01:50	OTH	+9.5/−5.0	−2.7	0.21	H
7	04/11/2006 22:30	RAD	+6.2/−8.4	+4.3	0.05	H
8	05/11/2006 17:50	RAD	+1.6/−13.1	−1.9	0.06	H
9	06/11/2006 17:30	STL	+1.3/−13.4	−12.1	0.18	H
10	07/11/2006 18:10	STL	+2.0/−12.8	−8.8	0.09	H
11	*08/11/2007 07:00	STL	−9.2/+0.0	+0.7	0.32	T
12	29/11/2006 20:20	RAD	+4.5/−11.1	+3.0	0.07	H
13	30/11/2006 12:20	STL	−3.5/+4.8	−10.7	0.11	H
14	03/12/2006 00:50	STL	+9.0/−6.7	−6.1	0.58	L
15	14/12/2006 18:00	RAD	+2.2/−13.7	−9.9	0.09	H
16	*15/12/2006 01:30	RAD	+9.7/−6.2	−5.7	0.39	H
17	*15/12/2006 02:30	STL	+10.7/−5.2	+2.3	0.09	H
18	16/12/2006 21:50	RAD	+6.0/−9.9	−7.6	0.07	T
19	18/12/2006 02:50	STL	+11.0/−4.9	−1.9	0.20	H
20	*18/12/2006 07:30	STL	+15.7/−0.3	+4.4	0.15	H
21	24/12/2006 04:10	STL	+12.3/−3.7	−2.3	0.23	H
22	25/12/2006 18:50	STL	+2.9/−13.0	−4.7	0.20	H
23	28/12/2006 01:50	STL	+9.9/−6.0	−4.5	0.71	H
24	28/12/2006 16:00	STL	+0.1/−15.8	−3.7	0.15	H
25	29/12/2006 05:00	STL	+13.1/−2.8	−0.8	0.71	T
26	07/01/2007 07:10	ADV	+15.1/−0.7	+0.2	0.45	T
27	27/01/2007 07:50	STL	−8.7/+0.3	+3.9	0.14	H
28	27/01/2007 23:30	RAD	+7.0/−8.1	−3.7	0.07	H
29	02/02/2007 10:00	OTH	−6.7/+2.5	+6.4	0.88	H
30	08/02/2007 02:20	PCP	+9.5/−5.0	−3.0	0.35	L
31	18/02/2007 22:40	RAD	+5.5/−8.4	+2.1	0.07	H
32	04/03/2007 06:30	RAD	+13.0/−0.1	+0.6	0.15	T
33	08/03/2007 07:00	ADV	−10.6/+0.5	+2.0	0.14	H
34	13/03/2007 23:10	RAD	+5.4/−7.1	+1.4	0.10	H
35	16/03/2007 07:10	MTR	−10.7/+1.0	+3.6	0.07	H
36	25/03/2007 03:10	OTH	+9.1/−2.7	+0.6	0.58	T

Table 4. Summary of quasi-fog events, with the date and time of the beginning of the event, local weather conditions (SKC: clear sky, PCP: presence of precipitation, LowC: presence of low clouds, MidC: presence of midlevel clouds), duration, the minimum visibility observed during the event, and synoptic weather classification (H: anticyclonic, L: cyclonic, T: transition).

No.	Date/time (day/month/year h:min)	Local weather conditions	Duration (h)	Lowest visibility (km)	Synoptic weather
1	29/10/2006 07:50	LowC	2.5	1.53	H
2	29/10/2006 22:00	SKC	9.7	1.05	H
3	30/10/2006 21:30	MidC	2.5	1.22	H
4	03/11/2006 00:10	SKC	7.3	1.39	H
5	04/11/2006 18:50	SKC	2.5	1.25	H
6	13/12/2006 16:10	LowC	3.0	0.76	H
7	16/12/2006 03:20	LowC	3.2	1.70	T
8	18/12/2006 23:20	SKC	8.2	1.82	H
9	26/12/2006 05:10	LowC	5.0	1.76	H
10	06/01/2007 02:10	PCP+LowC	0.8	1.92	L
11	29/01/2007 19:20	SKC	14.5	1.82	H
12	01/02/2007 02:10	LowC	9.8	1.31	H
13	05/02/2007 21:00	LowC	15.0	1.99	T
14	07/02/2007 03:30	LowC	8.0	0.85	T
15	19/02/2007 20:10	SKC	13.3	0.40	H
16	02/03/2007 18:00	PCP+LowC	3.2	1.86	H
17	09/03/2007 10:20	PCP+LowC	1.3	1.78	L
18	11/03/2007 03:50	SKC	3.2	1.41	H
19	27/03/2007 00:20	SKC	8.3	1.58	L
20	27/03/2007 23:00	SKC	9.8	1.60	T
21	29/03/2007 03:10	SKC+LowC	10.0	1.12	L

of fog, not long enough to be considered as significant fog events. Light precipitation also contributed to the reduction in visibility in three other quasi-fog cases, adding to the complexity in the nature of the observed low ceiling and visibility events.

The IOPs and their main characteristics are indicated in Fig. 4 and listed in Table 5. A significant variability in the type of situations was sampled, from the point of view of the occurrence of fog and near-fog conditions, as well as type, length, and intensity of fog events. For instance, several consecutive days of anticyclonic weather in March 2007 were characterized by several near-fog events, including a quasi-fog event (IOP 14), followed shortly by a long-lived dense radiation fog event (IOP 15). Both IOPs represent an opportunity to investigate the similarities, but more importantly the contrasting processes, that culminated in the formation of fog in one case (IOP 15) and its absence in the other (IOP 14). Both cases were characterized by weak winds, surface radiative cooling, and significant aerosol loads with particle concentrations around 10,000 cm^{-3}. More subtle contrasts in local and/or mesoscale dynamical processes, rather than aerosol characteristics, were

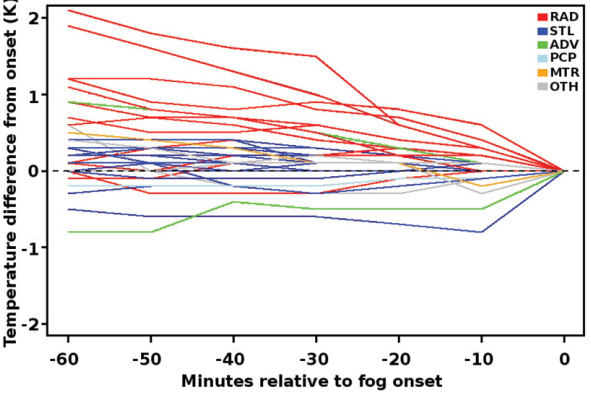

Fig. 5. Evolution of 2-m temperature, normalized with respect to temperature at fog onset, over the 60 minutes prior to fog formation, for individual events discriminated by type (color legend).

Table 5. Summary of the IOPs, including the date and time of the beginning of the event, the type of event (with fog type when relevant), event duration, lowest visibility observed during the night, and associated synoptic weather classification (H: anticyclonic, L: cyclonic).

IOP	Date (day/month/year)	Type of event and fog type	Duration (h)	Lowest visibility (km)	Synoptic weather
0	07–08/11/2006	Fog (STL)	4.7	0.09	H
1	29–30/11/2006	Fog (RAD)	14.2	0.07	H
2	14–15/12/2006	Fog (RAD)	11.8	0.09	H
3	17–18/12/2006	Fog (STL)	7.7	0.20	H
4	19–20/12/2006	—	—	6.25	H
5	20–21/12/2006	Near fog	7.3	2.58	H
6	14–15/01/2007	Near fog	2.0	3.40	H
7	22–23/01/2007	—	—	8.09	L
8	27–28/01/2007	Fog (RAD)	4.3	0.70	H
9	30–31/01/2007	—	—	7.10	H
10	02–03/02/2007	Near fog	3.7	2.70	H
11	03–04/02/2007	—	—	6.71	H
12	14–15/02/2007	Near fog	1.5	3.69	H
13	18–19/02/2007	Fog (RAD)	10.5	0.07	H
14	10–11/03/2007	Near fog	3.2	1.41	H
15	13–14/03/2007	Fog (RAD)	8.5	0.10	H

Table 6. Observed distribution of aerosol number concentration (in cm^{-3}) in different weather and fog regimes.

		Aerosol number concentration (cm^{-3})		
Regime	Occurrence (% w.r.t. all situations)	Min	Max	Range of 75% of the distribution
Easterly (20°–160°)	25	2,000	30,000	7,000–22,000
Westerly (220°–320°) Wind speed < 5 s^{-1}	27.5	2,000	22,000	2,000–11,000
Westerly (220°–320°) Wind speed > 5 s^{-1}	22.5	1,000	16,000	1,000–6,000
Quasi fog	—	1,000	20,000	6,000–18,000
Onset of fog	—	2,000	25,000	—
During fog	—	2,000	12,000	4,000–8,000

likely responsible for the occurrence/absence of fog formation in these cases.

The aerosol number concentration (N_{aer}), measured by a condensation particle counter (CPC), ranged from 1,000 to 30,000 cm^{-3} during ParisFog. Wind speed and direction were identified as two main factors controlling the local aerosol concentration. The N_{aer} was largest under easterly conditions (25% of occurrences), as shown in Table 6, when the Paris area is exposed to continental air masses and the SIRTA observatory is in the Paris plume (Chazette et al. 2005). In 25% of easterly conditions, N_{aer} at SIRTA ranged between 15,000 and 22,000 cm^{-3}, similar to levels observed in the Po Valley in 1989 and 1994 by Noone et al. (1992) and Yuskiewicz et al. (1998), respectively. The N_{aer} were significantly less in westerly flow conditions (50% of occurrence) advecting oceanic air masses found upstream of Paris.

Fog and quasi-fog conditions occurred in weak to moderate wind (wind speed < 5 m s^{-1}), whatever the wind direction. Variable aerosol number concentrations were observed during quasi-fog events, ranging from 1,000 cm^{-3} (06/01) to more than 20,000 cm^{-3} (e.g., 06/02, 07/02, and 08/03), with 75% of the dis-

tribution ranging between 6,000 and 18,000 cm^{-3}. Variable aerosol conditions were also encountered at the onset of fog events, ranging from 2,000 cm^{-3} (07/01) to 25,000 cm^{-3} (08/03). In the presence of fog, however, 75% of the N_{aer} distribution ranged between 4,000 and 8,000 cm^{-3} because of collision of aerosols with hydrated aerosols and fog droplets and, to a lesser extent, activation of aerosols into fog droplets (e.g., Noone et al. 1992).

Aerosol samples were collected during ParisFog to monitor chemical composition of aerosols before, during, and after six major fog events. Samples were collected within two size fractions [fine mode with aerodynamic diameter (AD) < 2 μm and coarse mode with AD > 2 μm]. Mass concentration [particulate matter (PM)] determined by gravimetric measurements and chemical analyses of the major aerosol components (ions, carbon, crustals) were performed in these two size fractions using the sampling and analytical protocols reported by Sciare et al. (2005). Ammonium nitrate and ammonium sulfate were shown to represent on average 50% of PM in the fine mode, the rest being composed of carbonaceous material (black carbon and organic matter) for approximately 40% and sea salt and crustal material for less than 10%. The highest values of inorganic salts (ammonium nitrate and ammonium sulfate) were observed during stable conditions with low dispersion and preferentially during high pressure system periods with air masses of continental Europe origin, which are conditions favorable to nighttime radiative cooling in winter. This finding is consistent with those reported by Bessagnet et al. (2005), who suggested that a significant fraction of inorganic salts measured in the region of Paris may have a European rather than a regional origin. Periods with fog were characterized by a decrease in water soluble contents (mainly inorganic salts) and poorly affected carbonaceous aerosols, which are, during wintertime, mainly of primary origin (traffic) and thus poorly water soluble. Nitrate and sulfate aerosols have shown to be fully neutralized by ammonium even during the fog events.

ILLUSTRATING KEY PROCESSES INVOLVED IN STRATUS, RADIATIVE, AND QUASI-FOG EVENTS. This section discusses the temporal evolution of multiple parameters (e.g., temperature, humidity, visibility, longwave radiative flux, wind speed, and turbulent kinetic energy) and processes (e.g., radiative cooling rate, particle activation, turbulent mixing, and coupling) throughout the life cycle of three specific events encountered during ParisFog: stratus-lowering fog, radiative fog, and quasi fog.

Stratus-fog events: 23–29 December 2006. The 12-day period ranging from 17 to 29 December 2006 was characterized by a large high pressure system moving slowly eastward from England, over the North Sea toward Holland and France. After 5 days of mostly cloud-free skies, a low-altitude cloud deck appeared on 23 December, persisting through 29 December, at which point the high was replaced by a trough coming over northwest France extending from a low over the North Atlantic. During this 7-day period, the visibility was reduced below 5 km more than 75% of the time, while five fog events of "stratus-lowering type" occurred and lasted a total of about 25 h.

Figure 6 illustrates multiple transitions between stratus and fog layers based on near-surface horizontal visibility (Fig. 6a), cloud-base height derived from ceilometer backscatter profiles (Figs. 6a–c), and cloud radar vertical profiles of reflectivity (Fig. 6b) and vertical Doppler velocity (Fig. 6c) for the 23–29 December period. Figure 6b shows that the period was characterized by multiple events of cloud-base lowering followed by cloud-base rising with a stratus-fog layer ranging in depth from 200 to 1,000 m. Cloud radar reflectivity profiles up to 12 km (not shown) indicate that there were no clouds above the stratus deck during the entire period. Several processes have been suggested to explain variations in near-surface stratus cloud-base heights (e.g., Oliver et al. 1978; Pilié et al. 1979). ParisFog observations show that several processes were at play during the period. The first fog event (0400 UTC 24 December) was preceded by stratus base lowering coinciding with near-surface cooling and humidification in moderate turbulence near the surface induced by wind shear. Hence, turbulent coupling between the cloud and surface cooling conditions is a likely explanation of the lowering of cloud base. The fog event was short-lived and quickly followed by a rapid rise in visibility and cloud-base height that was, however, not phased with any surface heating but coincided with the onset of drizzle inside the cloud and below cloud base with fall velocities observed near 2 m s^{-1} (Fig. 6c). Depending on the intensity of sedimentation, drizzle is thought to either lower cloud-base height through evaporation leading to humidification and cooling of the subcloud layer, or, as observed here, lead to the transition of fog into an elevated stratus.

The next cloud-base drop occurred on 25 December from 0000 to 1900 UTC leading to an eight-hour fog event. This time, cloud base and cloud top dropped

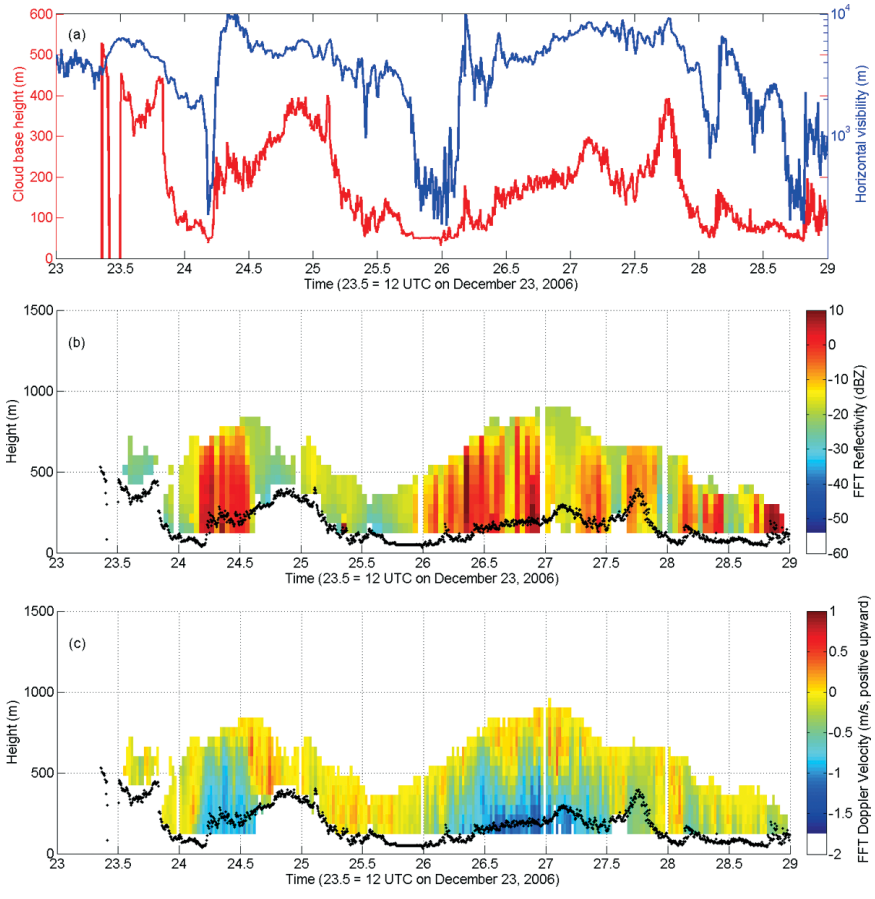

Fig. 6. Stratus-fog transitions during a 7-day period, 23–29 Dec 2006. (a) Visibility at the ground is shown in blue; cloud-base height is shown in red; 94-GHz cloud radar vertical profiles of (b) reflectivity in dBZ and (c) Doppler velocity in m s^{-1}.

steadily together, a phenomenon that could be explained by large-scale subsidence (e.g., Koračin et al. 2001). As near-surface temperature also dropped during this event, turbulent coupling could also explain the cloud-base lowering. Note that during this slow subsidence event, the mean in-cloud vertical velocities were near 0 m s^{-1} (Fig. 6c). This second fog event was followed by 36 h of 5–10-km visibility during which the cloud-base height progressively raised while the cloud thickened. This cloud-base rising was again coincident with a 24-h period of drizzle.

These observations show the complexity of the low cloud episode, suggesting that different processes were at play during the multiple stratus-lowering and rising phases of the event. Of particular interest are the conditions that trigger sedimentation, a major process removing condensed water. A more in depth analysis of microphysics, sedimentation, and turbulence in the stratus layer will be conducted in the near future using Doppler cloud radar retrievals of the liquid water content, extinction, droplet fall speed, and size (e.g., Protat et al. 2003) and 1D or large-eddy simulation (LES) numerical simulations.

A radiative fog event: 18–19 February 2007. On 18 February 2007, following two days of perturbed weather with light precipitation due to a trough moving eastward from the Atlantic, a weak ridge developed over France associated with a high pressure system centered over England. This condition induced a westerly flow under cloudless skies during daytime with a moderate aerosol load around 10,000 cm^{-3}, resulting in a maximum temperature of 15°C (Fig. 7a) and a maximum 30,000-m visibility (Fig. 7d) reached at 1500 UTC. Sunset (1700 UTC) was marked by a wind shift to the east advecting aerosols from the urban area with a wind speed of about 2 m s^{-1} at 10 m and 3.5 m s^{-1} at 30 m AGL (Fig. 7c), while the mixing layer depth started to decrease (ceilometer data not shown). At 1800 UTC radiative cooling of the near-surface layer reached a rate of –3 K h^{-1}, a typical rate that can lead to both stratification and supersaturation in the surface layer. At 1900 UTC, vertical stratification in the surface layer (surface to 30 m AGL) had reached 0.13°C m^{-1}. The number concentration N_{uf} of aerosol particles with diameter smaller than 0.05 μm had increased by a factor of 2 (from 8,000 to 17,000 cm^{-3}), while the number concentration N_{acc} of aerosol particles with diameter ranging between 0.05 and 2 μm had increased by a factor of 4 to reach 100 cm^{-3} (Elias et al. 2009). As a consequence, visibility had decreased by a factor of 3 to reach about 10,000 m.

During the following four hours (1900–2300 UTC) before fog onset, N_{acc} increased by a factor of 30 reaching 3,000 cm^{-3}, revealing the initiation of the hydration process under relative humidities greater than 80%, while N_{uf} remained around 19,000 cm^{-3}

because of a constant supply of aerosols. As a result of the hydration of aerosols, visibility decreased by another factor of 20. A brief cloud overpass created a destabilization effect significantly reducing stratification to 0.06°C m^{-1} until fog onset. At 2200 UTC the radiative cooling rate in the surface layer was significantly reduced, while the turbulent kinetic energy (TKE) reached a local minimum at both 10- and 30-m heights (Fig. 7f; TKE_{min} = 0.02 m^2 s^{-2}). In the next 20-min interval (2220–2240 UTC), fog droplets appeared as the liquid droplet concentration measured at 2-m height reached 100 cm^{-3}, causing a sudden increase in particle surface area, an essential parameter governing the interaction between particles and radiation. In that time interval, the radiative cooling rate increased to –3 K h^{-1} in a shallow layer decoupled from the rest of the surface layer (Fig. 8; 1- and 2-m temperature sensors). At 2245 UTC, the rate of change in visibility reached a maximum as the visibility dropped below 600 m. In the next 30 minutes (2245–2315 UTC), the 1- and 2-m temperature sensors showed an increase at a rate reaching +5 K h^{-1}. As a result, the stable structure of the surface layer quickly changed to a neutral lapse rate. Thermal homogenization of the surface layer was due to radiative cooling at the top of the growing fog layer destabilizing the layer inducing turbulent mixing, as well as emission and absorption of infrared radiation by fog droplets. TKE reached a local maximum at 10 and 30 m AGL near 2300 UTC (0.25 m^2 s^{-2} < TKE_{max} < 0.45 m^2 s^{-2}), a phenomenon that was also observed during the radiative fog event of 27–28 January 2007.

A tethered balloon carrying five temperature, humidity, and wind sondes was installed to monitor conditions at about 50, 75, 95, 115, and 130 m AGL. Figure 8 shows the temporal evolution of temperatures at 10 levels from 1 m up to 140 m AGL. At 2300 UTC thermal homogenization occurred over

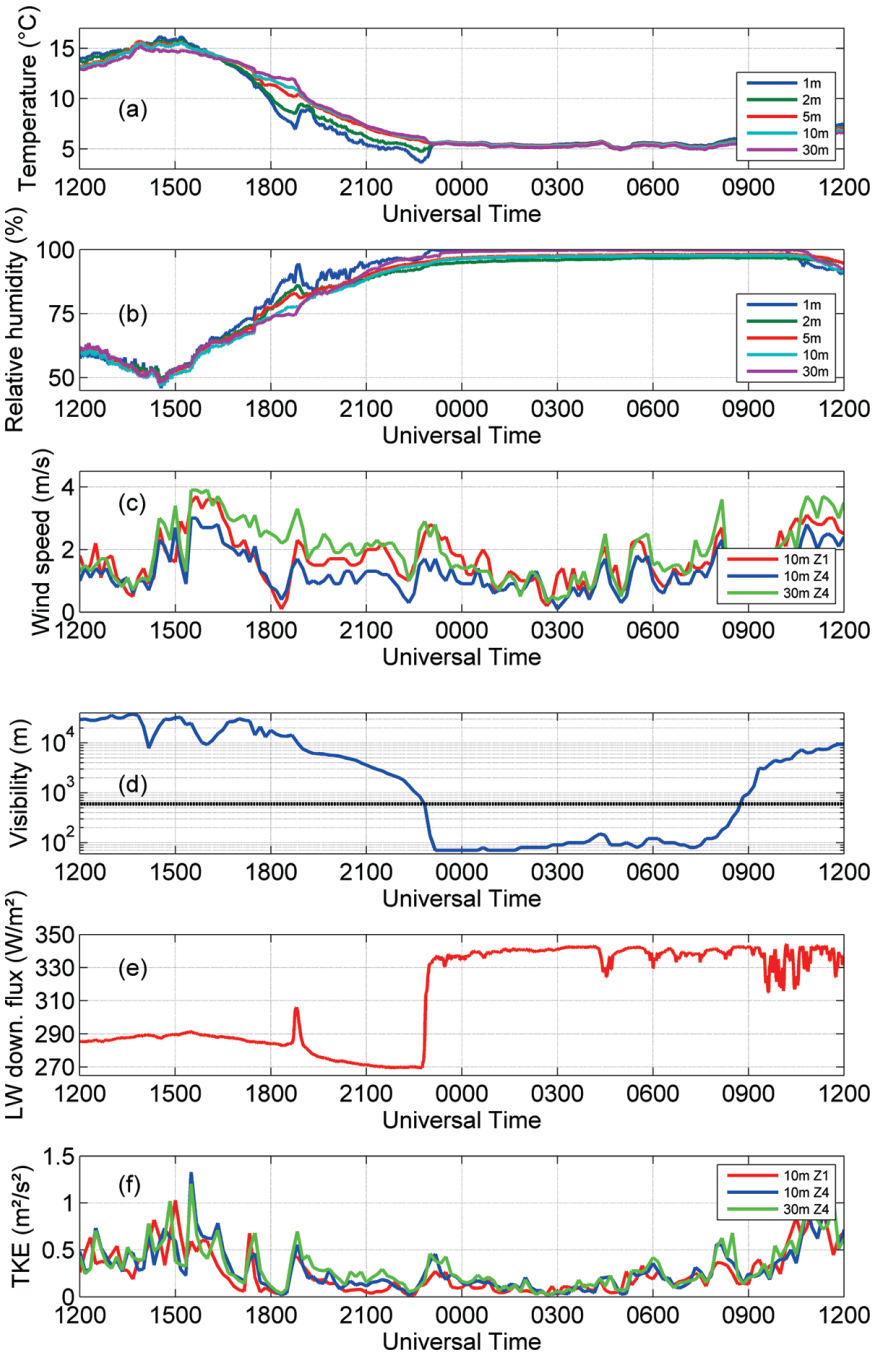

Fig. 7. Twenty-four-hour diurnal cycle on 18–19 Feb 2007 of (a) near-surface temperature, (b) near-surface relative humidity, (c) wind speed, (d) visibility, (e) downwelling longwave irradiance, and (f) turbulent kinetic energy.

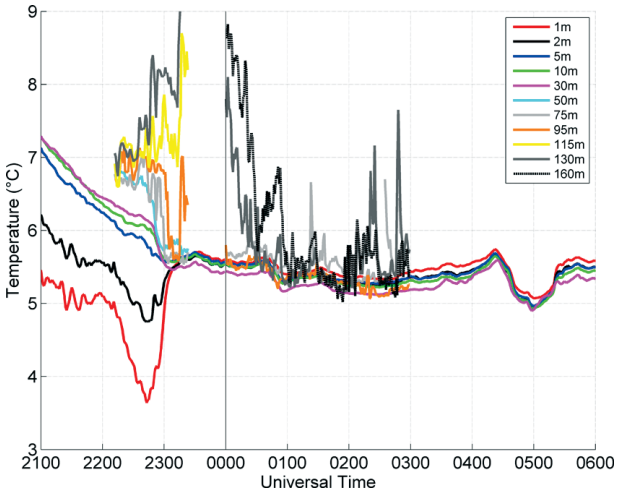

Fig. 8. Evolution of the temperature vertical profile from ground to 160 m, measured from temperature sensors deployed on a 30-m mast and a tethered balloon, during the night of 18–19 Feb 2007. The tethered balloon is deployed from 2215 UTC until 2315 UTC and from 0000 UTC until 0300 UTC.

a 75-m-deep layer at about +5.5°C; 15 min later the neutral layer reached 95 m. At that time, the 115- and 130-m temperatures showed a 1° and 2°C temperature inversion, respectively, indicating that the top of the fog layer was near 95 m. At 2315 UTC, the tethered balloon was raised 20 m to improve its floatability; the 95-m sonde temperature jumped +1.5°C as it reached 115 m. This behavior confirmed the altitude of the temperature inversion. The balloon was lowered to the ground at 2330 UTC and redeployed at 0000 UTC with only four sondes (at 75, 95, 130, and 160 m) to improve its floatability. The temperature time series of Fig. 8 shows that the fog layer reached 130 m at 0030 UTC and 160 m at 0100 UTC and reveals that the radiative cooling rate at the top of the fog layer reached about -6 K h^{-1}.

The dense fog lasted more than nine hours, with visibility varying between 50 and 200 m in a fog layer 200–300 m thick (from radiosonde data, not shown). The fog event ended, at 0845 UTC on 19 February about two hours after sunrise, as cloud base lifted from the ground. This episode illustrates the interactions between radiative cooling rate, turbulent mixing, and aerosol activation under high relative humidity (supersaturation) and shows the potential for ParisFog data to support more detailed numerical investigations (e.g., Rangognio et al. 2009) of such interactions.

A quasi-fog event: 18–19 December 2006. Twenty-one quasi-fog situations appear in the ParisFog classification, with about 50% under radiative cooling conditions, that is, clear-sky conditions. Here we discuss the situation observed on the night of 18–19 December 2006.

The large-scale situation leading to this quasi-fog condition was a large high pressure system over the eastern Atlantic and western Europe. Daytime 18 December was characterized by a near-surface stratus layer that began rising at 1400 UTC and dissipated around 2000 UTC leaving a perfectly cloudless sky during the night of 18–19 December (ceilometer data, not shown). At 2000 UTC, the relative humidity was already at 80% in a neutral surface layer. Wind speed was about 2 m s^{-1}, as radiative cooling of the surface layer began, and conditions appeared to be favorable for fog formation (Figs. 9a–c).

As expected in clear-sky conditions, the near-surface temperature dropped because of radiative cooling, reaching cooling rates peaking at -6 K h^{-1} around 2100 UTC, and the surface layer quickly became stably stratified. This cooling, however, only lasted four hours, after which the surface layer transitioned to a neutral lapse rate (Fig. 9a). Significant turbulence with a TKE exceeding 1 m^2 s^{-2} (Fig. 9f) appeared after 0000 UTC, possibly explained by wind shear between 10 and 30 m AGL (Fig. 9c), which is a likely explanation for the thermal neutralization of the surface layer after midnight, with a positive feedback as less stratified layers are more subject to turbulence.

Visibility dropped to about 3 km at midnight, indicating a significant load of hydrated aerosols that never activated to cloud droplets. Between 0400 and 0600 UTC on 19 December, enhanced incoming IR radiation associated with the appearance of a cloud deck at 200–300 m in altitude may explain the transition to a neutral stratification of the surface layer. As several processes inhibited the radiative cooling of the surface layer during the night, the relative humidity was not able to rise to the supersaturation needed to activate fog droplets. This example illustrates very well the complexity of a situation that was forecast as favorable for fog formation but during which small-scale turbulence counteracted the radiative cooling, ultimately preventing supersaturation and hence inhibiting the formation of fog droplets.

CONCLUSIONS. The ParisFog field experiment was carried out in winter 2006/07 at the SIRTA observatory to monitor simultaneously thermodynamic, dynamic, and turbulent microphysical and radiative processes, and chemical composition of aerosols, in low-visibility situations occurring in a large range of

synoptic conditions. The ParisFog dataset now contains 3,000 h of measurements, including over 100 events of fog and near fog, with a particular focus on 21 distinct quasi-fog situations. Ten such situations occurred under cloudless skies, with relative humidities and radiative cooling rates similar to those observed at the onset of fog events, but did not lead to droplet activation and fog formation. To understand what process or processes prevented droplet activation in spite of intense radiative cooling, ParisFog data are available to study if turbulent mixing or aerosol number concentrations exceeding critical values could explain the phenomenon, as suggested in numerical studies performed by Rangognio et al. (2009).

Another unique feature of the ParisFog dataset is a 7-day-long oscillation between low stratus and fog. This event was monitored continuously by a visibility meter, a ceilometer, a 95-GHz Doppler cloud radar, surface weather and radiation sensors, near-surface sonic anemometers, and radiosonde profiles performed twice daily. Preliminary analysis of this situation revealed that turbulent coupling between surface conditions and cloud base could explain the multiple descending motions of cloud base leading to low-visibility fog conditions during that week. Cloud radar monitoring of cloud top also suggested the possible influence of large-scale dynamical processes modulating the subsidence in the lower free troposphere. Furthermore, radar Doppler velocities revealed that two distinct fog dissipation events were likely triggered by the onset of significant in-cloud particle sedimentation velocity, both occurring in the early morning hours several hours before sunrise. As sedimentation flux is a major factor controlling loss of condensed water, as suggested in a single-column model study by Zhang et al. (2010), this long stratus event could be suited for testing parameterizations of droplet settling velocity and exploring the conditions that triggered sedimentation.

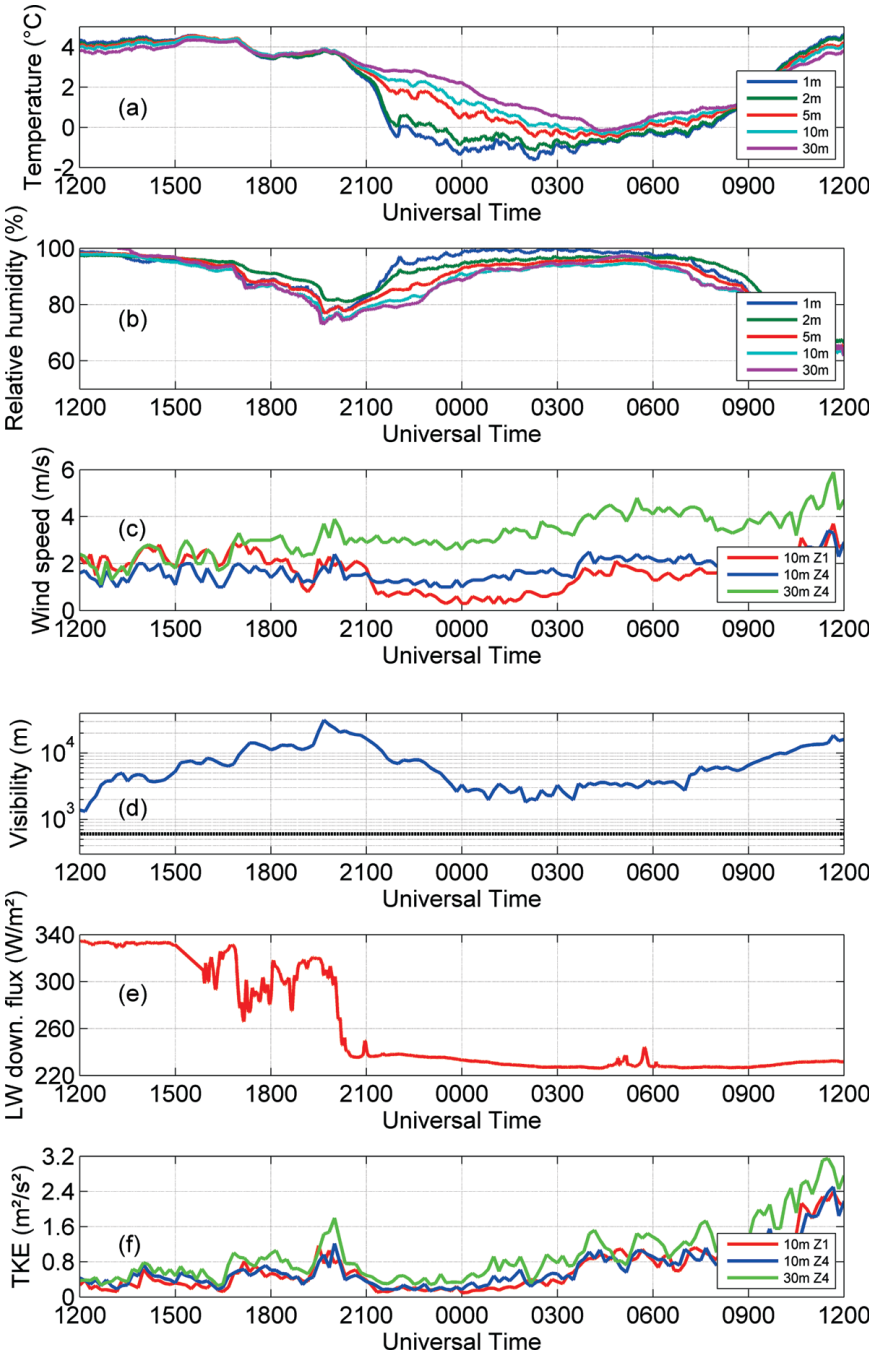

Fig. 9. Twenty-four-hour diurnal cycle on 18–19 Dec 2006 of (a) near-surface temperature, (b) near-surface relative humidity, (c) wind speed, (d) visibility, (e) downwelling longwave irradiance, and (f) turbulent kinetic energy.

The ParisFog dataset also contains a few radiative fog events where the aerosol and fog droplet size distributions and number concentrations were characterized. Those events are particularly suited to enhance our understanding of the balance between infrared radiative cooling rates and turbulent mixing that are at play at fog onset in the positive feedback loop where radiative cooling leads to supersaturation, which in turn leads to aerosol activation into cloud droplets, which in turn enhances radiative cooling at the top of the fog layer, and so on. As shown by Elias et al. (2009), hydrophilic aerosols reach large sizes under very high relative humidities and hence reduce horizontal visibility to near 1 km. ParisFog infrared irradiance measurements and infrared radiative transfer calculations could be used to quantify how these large aerosols affect the radiative cooling rate and to pin down if turbulent mixing is enhanced as a result of droplet activation or acts as a trigger of droplet activation. The ParisFog database is available for scientific research and open to scientists worldwide to pursue exploring these questions.

ACKNOWLEDGMENTS. The ParisFog field experiment was supported by the Centre National de la Recherche Scientifique (CNRS), Institut National des Sciences de l'Univers (INSU), Météo-France, Electricité de France (EDF), Délégation Générale pour l'Armement (DGA), and Ecole Polytechnique. The authors would like to acknowledge over 60 participants that contributed to the realization of this field experiment from the following institutes and laboratories: Centre National de Recherche en Météorologie (CNRM), Institut Pierre Simon Laplace (IPSL), Centre d'Enseignement et de Recherches en Environnement Atmosphérique (CEREA), Centre d'Etudes des Environnements Terrestres et Planétaires (CETP), Laboratoire de Météorologie Dynamique (LMD), Laboratoire des Sciences du Climat et de l'Environnement (LSCE), Laboratoire Régional des Ponts et Chaussées (LRPC), Institut de Physique du Globe de Paris (IPGP), Service d'Aéronomie (SA), and Service Hydrographique et Océanographique de la Marine (SHOM).

REFERENCES

Bergot, T., 2007: Quality assessment of the Cobel-Isba numerical forecast system of fog and low clouds. *Pure Appl. Geophys.,* **164,** 1265–1282.

——, D. Carrer, J. Noilhan, and P. Bougeault, 2005: Improved site-specific numerical prediction of fog and low clouds: A feasibility study. *Wea. Forecasting,* **20,** 627–646.

——, and Coauthors, 2008: Paris-FOG: Des chercheurs dans le brouillard. *La Météor.,* **62,** 48–58.

Bessagnet, B., A. Hodzic, O. Blanchard, M. Lattuati, O. Le Bihan, H. Marfaing, and L. Rouil, 2005: Origin of particulate matter pollution episodes in wintertime over the Paris Basin. *Atmos. Environ.,* **39,** 6159–6174.

Chazette, P., H. Randriamiarisoa, J. Sanak, P. Couvert, and C. Flamant, 2005: Optical properties of urban aerosol from airborne and ground based in situ measurements performed during the Etude et Simulation de la Qualité de l'air en Ile de France (ESQUIF) program. *J. Geophys. Res.,* **110,** D02206, doi:10.1029/2004JD004810.

Croft, P. J., R. L. Pfost, J. L. Medlin, and G. A. Johnson, 1997: Fog forecasting for the southern region: A conceptual model approach. *Wea. Forecasting,* **12,** 545–556.

Delanoë, J., A. Protat, D. Bouniol, A. J. Heymsfield, A. Bansemer, and P. Brown, 2007: The characterization of ice clouds properties from Doppler radar measurements. *J. Appl. Meteor. Climatol.,* **46,** 1682–1698.

Duynkerke, P. G., 1991: Radiation fog: A comparison of model simulation with detailed observations. *Mon. Wea. Rev.,* **119,** 324–341.

——, 1999: Turbulence, radiation and fog in Dutch stable boundary layers. *Bound.-Layer Meteor.,* **90,** 447–477.

Elias, T., and Coauthors, 2009: Particulate contribution to extinction of visible radiation: Pollution, haze, and fog. *Atmos. Res.,* **92,** 443–454.

Fuzzi, S., and Coauthors, 1992: The Po Valley Fog Experiment 1989: An overview. *Tellus,* **44B,** 448–468.

——, and Coauthors, 1998: Overview of the Po Valley fog experiment 1994 (CHEMDROP). *Contrib. Atmos. Phys.,* **71,** 3–19.

Glickman, T., Ed., 2000: *Glossary of Meteorology.* 2nd ed. Amer. Meteor. Soc., 855 pp.

Guédalia, D., and T. Bergot, 1994: Numerical forecasting of radiation fog. *Mon. Wea. Rev.,* **122,** 1218–1230.

Guidard, V., and D. Tzanos, 2007: Analysis of fog probability from a combination of satellite and ground observation data. *Pure Appl. Geophys.,* **164,** 1207–1220.

Gultepe, I., and Coauthors, 2007: Fog research: A review of past achievements and future perspectives. *Pure Appl. Geophys.,* **164,** 1121–1159.

Haeffelin, M., and Coauthors, 2005: SIRTA, a ground-based atmospheric observatory for cloud and aerosol research. *Ann. Geophys.,* **23,** 253–275.

Ivaldi, C., D. A. Clark, and D. Reynolds, 2006: Upgrade and technology transfer of the San Francisco Marine Stratus Forecast System to the National Weather Service. Preprints, *12th Conf. on Aviation, Range and Aerospace Meteorology,* Atlanta, GA, Amer. Meteor. Soc., P1.16.

Koračin, D., J. Lewis, W. T. Thompson, C. E. Dorman, and J. A. Businger, 2001: Transition of stratus into fog along the California coast: Observations and modeling. *J. Atmos. Sci.,* **58,** 1714–1731.

Météo-France, cited 2008: Nombre annuel de jours de brouillards par ville en France (calculé sur la période 1971–2000) [Annual number of fog days per city in France (over the 1971–2000 period)]. [Available online at http://france.meteofrance.com/content/2008/4/3390-48.pdf.]

Meyer, M. B., and G. G. Lala, 1990: Climatological aspects of radiation fog occurrence at Albany, New York. *J. Climate,* **3,** 577–586.

——, ——, and J. E. Jiusto, 1986: FOG-82: A cooperative field study of radiation fog. *Bull. Amer. Meteor. Soc.,* **67,** 825–832.

Noone, K. J., and Coauthors, 1992: Changes in aerosol size and phase distributions due to physical and chemical processes in fog. *Tellus,* **44B,** 489–504.

Oliver, D. A., W. S. Lewellen, and G. G. Williamson, 1978: The interaction between turbulent and radiative transport in the development of fog and low-level stratus. *J. Atmos. Sci.,* **35,** 301–316.

Pilié, R. J., E. J. Mack, C. W. Rogers, U. Katz, and W. C. Kockmond, 1979: The formation of marine fog and the development of fog-stratus systems along the California coast. *J. Appl. Meteor.,* **18,** 1275–1286.

Protat, A., Y. Lemaitre, and D. Bouniol, 2003: Terminal fall velocity and the FASTEX cyclones. *Quart. J. Roy. Meteor. Soc.,* **129,** 1513–1535.

Rangognio, J., P. Tulet, T. Bergot, L. Gomes, O. Thouron, and M. Leriche, 2009: Influence of aerosols on the formation and development of radiation fog. *Atmos. Chem. Phys. Discuss.,* **9,** 17 963–18 019.

Roach, W., 1995: Back to basics: Fog: Part 2—The formation and dissipation of land fog. *Weather,* **50,** 80–84.

——, R. Brown, S. J. Caughey, J. A. Garland, and C. J. Readings, 1976: The physics of radiation fog: I-A field study. *Quart. J. Roy. Meteor. Soc.,* **102,** 313–333.

Sciare, J., K. Oikonomou, H. Cachier, N. Mihalopoulos, M. O. Andreae, W. Maenhaut, and R. Sarda-Estève, 2005: Aerosol mass closure and reconstruction of the light scattering coefficient over the Eastern Mediterranean Sea during the MINOS campaign. *Atmos. Chem. Phys.,* **5,** 2253–2265.

Tardif, R., and R. M. Rasmussen, 2007: Event-based climatology of fog in the New York City region. *J. Appl. Meteor. Climatol.,* **46,** 1141–1167.

——, and ——, 2008: Process-oriented analysis of environmental conditions associated with precipitation fog events in the New York City region. *J. Appl. Meteor. Climatol.,* **47,** 1681–1703.

Wobrock, W., and Coauthors, 1992: Meteorological characteristics of the Po Valley fog. *Tellus,* **44B,** 469–488.

Yiou, P., R. Vautard, P. Naveau, and C. Cassou, 2007: Inconsistency between atmospheric dynamics and temperatures during the exceptional 2006/2007 fall/winter and recent warming in Europe. *Geophys. Res. Lett.,* **34,** L21808, doi:10.1029/2007GL031981.

Yuskiewicz, B., and Coauthors, 1998: Changes in submicrometer particle distributions and light scattering during mist and fog events in a highly polluted environment. *Contr. Atmos. Phys.,* **71,** 33–45.

Zhang, X., L. Musson-Genon, B. Carissimo, and E. Dupont, 2010: Numerical sensitivity analysis of a radiation fog event with a single-column model. *J. Appl. Meteor. Climatol.,* in press.

SHOP

the new AMS online bookstore

Use this **easy-to-navigate** site to review and purchase new and classic titles in the collection of AMS Books—including general interest weather books, histories, biographies, and monographs—plus much more.

View tables of contents, information about the authors, and independent reviews.

As always, **AMS members receive deep discounts** on all AMS Books.

www.ametsoc.org/amsbookstore

The new AMS online bookstore is now open.

Booksellers and wholesale distributors may set up accounts with our distributor, The University of Chicago Press, by contacting Karen Hyzy at khyzy@press.uchicago.edu, 773-702-7000, or toll-free at 800-621-2736.

AMS BOOKS

RESEARCH | APPLICATIONS | HISTORY